Advances in Science and Technology Research Journal

Advances in Science and Technology Research Journal 2023, 17(1), 315–331
https://doi.org/10.12913/22998624/159070
ISSN 2299-8624, License CC-BY 4.0

Received: 2022.11.22
Accepted: 2023.01.17
Published: 2023.02.01

Experimental and Numerical Characterization of Thermal Bridges in Windows

Robert Smusz[1], Paweł Bałon[2,3*], Bartłomiej Kiełbasa[3], Edward Rejman[1], Michał Bembenek[2], Łukasz Kowalski[2]

[1] Rzeszow University of Technology, Al. Powstańców Warszawy 12, 35–959 Rzeszów, Poland
[2] Faculty of Mechanical Engineering and Robotics, AGH University of Science and Technology, al. A. Mickiewicza 30, 30-059 Krakow, Poland
[3] F.H.U. ATUT Marek i Alicja Janeczek, ul. Kościuszki 56, 39-300 Mielec, Poland
* Corresponding author's e-mail: balonpawel@gmail.com

ABSTRACT

Actions aimed at improving the energy performance of buildings increase the share of heat loss through thermal bridges and windows in a building's energy balance. This is especially true of buildings currently under construction. In addition, it is known that the correct installation of windows is one of the biggest obstacles that must be overcome in order to achieve higher energy efficiency and reduce the impact of linear thermal bridges. Therefore, the study analysed, numerically and experimentally, the energy properties of PVC window frames with improved metal stiffening profiles, which were introduced to reduce the risk of window frame deformation and reduce leakage caused by faulty installation. The value of the frame thermal transmittance coefficient and the linear heat transfer coefficients were determined numerically. The simulation results showed that filling large air spaces with insulation material allowed for the reduction of the U_f frame's thermal transmittance coefficient by over 10%. Moreover, where the window connects with the wall, there was a reduction in the linear thermal bridges' influence on heat losses. The reduction in the linear thermal transmittance coefficient Ψ was 9.6%, 1.0%, and 3.5% for the window sill, jamb, and lintel, respectively, compared to a frame without insulation. Moreover, experimental studies were conducted on the influence of the insulation of the PVC window frame with metal closed stiffening profiles on the linear thermal bridge located at the joint with the glass. It was found that the incidence factor I_{tb} decreased by more than 6%. Thus, there is also a positive effect on the linear thermal bridge at the joint of the glass pane with the window frame.

Keywords: window frames; window construction, thermal bridges; thermography.

INTRODUCTION

In European Union countries, buildings are responsible for the consumption of 28% of final energy [1]. Natural gas consumption in this sector is significant and amounts to 36% [1]. Moreover, due to the growing population, it is predicted [2] that by 2050 there will be a 50% increase in energy demand in this sector of the economy. In addition, two-thirds of the European building stock was built before 1980 and has the low energy efficiency. These factors, along with the depletion of non-renewable energy sources and the cumulative risks and effects of climate change, have resulted in increasing measures being taken to reduce energy consumption. As a result, the EU has undertaken a number of legal initiatives to improve energy efficiency, including the energy performance of buildings. These activities have included the implementation of the Energy Performance of Buildings Directive [3], modified in 2018 [4], along with its revision in 2021. In light of these assumptions, the implementation of the Nearly Zero Energy Buildings (NZEB) model in Europe became mandatory on December 31, 2018 for new public buildings, and for all new

buildings starting on December 31, 2020. This made national regulations more stringent and the vast majority of countries associated with the United Nations Economic Commission for Europe (UNECE) already have formal requirements for energy efficiency standards in buildings [5]. Depending on the climatic conditions, the *U*-value of external partitions ranges from 0.15 W/m^{2}K to 0.30 W/m^{2}K [6], and for windows it ranges from 1 W/m^{2}K to 1.5 W/m^{2}K [7]. In Poland, in accordance with the regulations in force from December 31, 2020 for the temperature in rooms kept above 16°C [8], the maximum thermal transmittance coefficient for buildings should not exceed the following values: for external walls, 0.2 W/m^{2}K; for windows and balcony doors 0.9 W/m^{2}K, 1.1 W/m^{2}K for roof windows; 0.15 W/m^{2}K for roofs, and 1.3 W/m^{2}K for external doors. Actions aimed at improving the energy performance of buildings increased the share of heat loss through thermal bridges and windows in the building's energy balance. For example, for unrenovated buildings from the 70's, the share of thermal bridges in heat loss is 2–7% [9, 10], and for renovated and insulated buildings it rises to 17% [9]. On the other hand, for modern low-energy buildings built in Europe in moderate climate conditions (Dfb) [11] they do not exceed 8% [17]. On the other hand, for the Mediterranean climate (Csa) [11], [12] it was found that reducing the impact of thermal bridges is a very effective means to reduce primary energy demand, and the average annual energy savings are around 8.5%. Windows are one of the most important elements of buildings and play a key role not only in illuminating building interiors with daylight [13], but also in shaping the overall energy demand.

Traditional (regular) glass window panes are typically the coldest area in buildings. On the other hand, in windows with low-emission panes, the coldest place, which also has the greatest risk of moisture condensation, are the joints between the pane and the window frame [14], Fig. 1a. Moreover, windows are responsible for about 30% of heat loss from a building [15], but for low energy buildings this loss can reach higher values due to the large proportion of window area in relation to wall area. On the other hand, for a hot climate, linear thermal bridges have a significant impact on the energy demand for cooling a building [16]. Therefore, one way to effectively reduce heat loss in new buildings and renovate old buildings is to use new, energy-efficient windows and radically reduce the impact of linear thermal bridges. This also requires the correct installation of windows. Experience shows that the correct installation of windows is still one of the most difficult obstacles that must be overcome in order to achieve higher energy efficiency in buildings and reduce the influence of linear thermal bridges [18]. This is important because heat losses through linear thermal bridges at the connection of windows with walls may constitute up to 40% of heat losses from all thermal bridges in the building [19].

The problem that results from faulty window installation and the low torsional stiffness of PVC window profiles are leaks caused by frame deformation, Fig. 1b. This can also result from the use of open steel profiles that stiffen PVC window frames, the stiffness of which is many times lower than closed metal profiles. It should also be emphasized that a window frame deformed during cannot be repaired.

The thermal transmittance coefficient of the window joinery is still much higher than for external walls [15, 20, 21] which is the syntax for actions to reduce it [22, 23, 24] and it is also forced by the legal requirements related to the

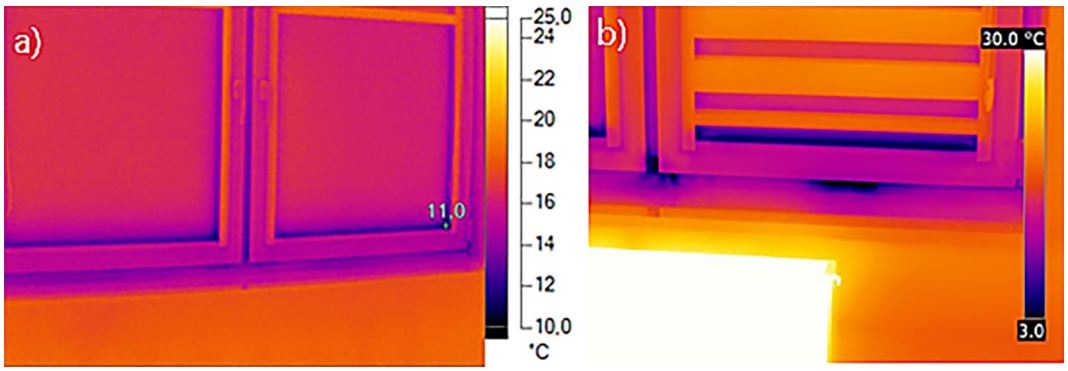

Fig. 1. Linear thermal bridges and leaks: (a) thermal bridge on joint of PVC frame and glazing; (b) window frame deformation and air leakage

tightening of formal energy efficiency standards in buildings [25, 26].

The weakest points of the window in terms of its thermal characteristics are the window frame and the linear thermal bridge that is formed at the pane-frame connection and the cable-type thermal bridge at the window-wall connection.

The thermal transmittance coefficient of the window frame depends on many factors, including the geometry, dimensions of the recesses and the emissivity of the surface [24, 27]. On the other hand, the value of heat loss through the linear thermal bridge at the connection between the window and the wall depends on the structure of the internal window frame, the wall structure, the location of the thermal insulation layer, the location of the window in relation to the wall and the quality of workmanship [28, 29, 30].

In order to reduce the risk of deformation of the window, it is very important to obtain high strength parameters. This is due to the fact that the window frame made of PVC has a very low torsional stiffness. However, nowadays, open metal stiffening profiles are used, almost exclusively Fig 2a. It is true that closed profiles, Fig. 2b, are more expensive than open profiles. However, their undeniable advantage is that they show many times greater torsional stiffness compared to open profiles, which reduces the risk of frame deformation during installation and reduces leakage.

Based on the classical structural mechanics and hydrodynamic analogy [31], the torsional stiffness of closed profiles C_c can be expressed by:

$$C_c = 4\frac{G\,A_m^2}{\sum_{i=1}^{N}\frac{l_i}{d_i}} \tag{1}$$

where: $G = \frac{E}{2\cdot(1+\nu)}$ – shear modulus (Kirchhoff modulus),

E – Young modulus;

ν – Poisson's ratio,

A_m – the mean area enclosed within the boundary of the centerline of the closed profiles' thickness is shown shaded in Fig. 3,

l_i – length of a constant thickness profile segment,

d_i – thickness profile segment,

N – number of segments along the entire perimeter of the profile.

On the other hand on the basis Saint-Venant torsion theory and membrane analogy the torsional stiffness of open profiles C_o can be expressed by [31]:

$$C_o = \frac{1}{3}G\sum_{i=1}^{N} l_i\, d_i^3 \tag{2}$$

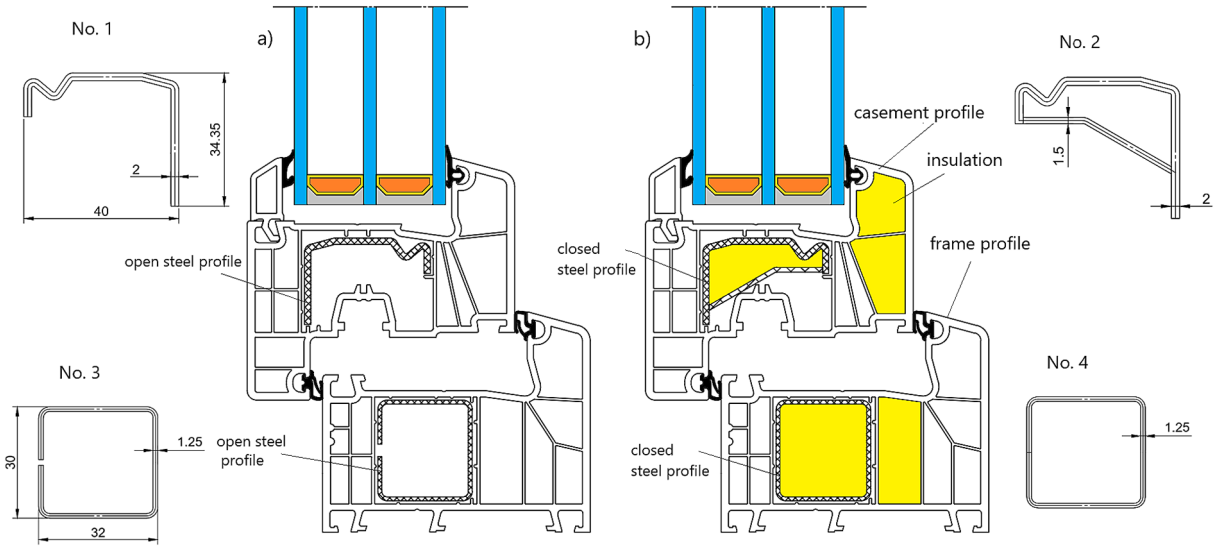

Fig. 2. Cross-section of the window frame analysed in the study (dimensions in mm):
a) PVC frame with open steel profile; b) PVC frame with closed steel profile and insulation

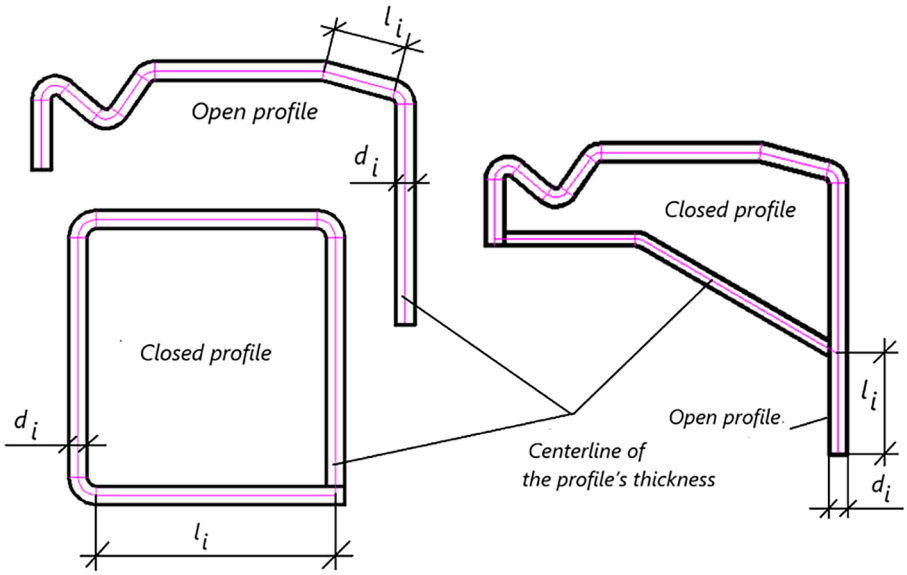

Fig. 3. Comparison between closed and open profiles

For structures composed of open and closed profiles, the torsional stiffness can be expressed as follows:

$$C = C_c + C_o \tag{3}$$

As can be seen (Table 1), closed profiles show much higher torsional stiffness in relation to open profiles (from several dozen to several hundred times greater). Therefore, it is advisable to use closed profiles.

In this study, an analysis was performed to determine the influence of additional thermal insulation on the thermal transmittance coefficient for window frames made of PVC, in which closed metal stiffening profiles were used in order to improve stiffness and reduce the risk of deformation during installation. Be aware that the use of closed metal stiffening profiles may have a negative effect on the thermal properties of the window frame. Therefore, additional insulation of the PVC frame was used. There have been many studies that focused on the influence of various window frame insulating materials [22, 24, 32] on the thermal characteristics of windows [33, 34, 35]. It has been shown in [35] that the use of polyurethane foam placed in large air cavities of PVC window frames can reduce the heat transfer coefficient by 10%. In turn, the authors of the work [34] managed to develop a window solution for which the thermal transmittance coefficient was 8.5% lower compared to a PVC window with a thermal transmittance coefficient of 0.7 W/m^{2}K. In the work [24] it was found that filling the air cavities of window frames with polyurethane foam can reduce the thermal transmittance coefficient of the frame by about 27%. The authors of the works [21, 22] used aerogel to fill recesses in the hollow profiles of PVC windows. The research [21, 22] shows that filling the hollow spaces (air-filled PVC cavities) in window frames with aerogel granules can reduce the thermal transmittance coefficient of the frame by up to 30%, depending on the frame's structure. However, the work presented above did not analyse the effect of closed stiffening profiles on the thermal characteristics of windows.

NUMERICAL EVALUATION OF THERMAL PERFORMANCE IN WINDOWS

Mathematical model and boundary conditions

In the first stage, the thermal transmittance coefficient of the window frame U_f was determined. The analysed window frames were modelled in accordance with the requirements contained in the standards [36, 39]. The steady state two-dimensional heat conduction through a window with convective boundary conditions was analysed. The numerical calculation of temperature field was used to determine frame thermal transmittance.

Table 1. Torsional stiffness analysis of the steel profiles (Young modulus E = 210 GPa and Poisson's ratio ν = 0.3)

No.	Torsional stiffness C, $[\frac{Nm}{rad}]$
1	16
2	1103
3	6
4	2700

In this case was solved the energy equation (Laplace's equation) for solid:

$$\frac{\partial^2 T}{\partial x^2} + \frac{\partial^2 T}{\partial y^2} = 0, \tag{4}$$

where: $T = T(x, y)$ is the temperature.

All of the solid body and fluid properties remained constant. Heat flow through PVC window frame air-filled cavities were modelled by means of heat conduction. The cavities were represented by equivalent thermal conductivity. This equivalent thermal conductivity coefficient includes the heat flow by conduction, convection and radiation and depends on the geometry of the cavity.

Perfect contact between adjacent materials was established. On the basis of energy balance and Fourier law for solid – solid interface, the heat flux density can be described:

$$k_i \frac{\partial T_i}{\partial n} = k_j \frac{\partial T_j}{\partial n} \tag{5}$$

where: n denotes the normal direction to the surface,
k_i, k_j the thermal conductivity of the adjacent materials.

The heat flux conditions for internal and external surfaces were given by Newton's law of convection.

For the internal side, Fig. 4:

$$-k \frac{\partial T}{\partial n} = h_{si}(T_i - T_{si}) \tag{6}$$

where: $h_{si} = \frac{1}{R_{si}}$ – heat transfer coefficient on the internal boundary,
T_i – indoor temperature,
T_{si} – surface temperature on the internal boundary of the model,
R_{si} – thermal surface resistance on the internal boundary of the model. And for external side, Fig. 4:

$$-k \frac{\partial T}{\partial n} = h_{se}(T_{se} - T_e), \tag{7}$$

where: $h_{se} = \frac{1}{R_{se}}$ – heat transfer coefficient, T_e – outdoor temperature, T_{se} – surface temperature on the external boundary of the model, R_{se} – thermal surface resistance on the external boundary of the model. Internal and external thermal surface resistances are not equal. Furthermore, on boundaries linked to the internal side, an increased thermal resistance according reduced radiation/convection in edges or junctions between two surfaces (corners) in accordance with [36]. An adiabatic conditions $\frac{\partial T}{\partial n} = 0$ at the other walls were assumed. Heat loss analysis and identification of the thermal transmittance coefficient were carried out using the finite element method. Numerical simulations were made using the commercial software COMSOL Multiphysics.

Frame geometrical model

In order to determine the thermal transmittance coefficient U_f of the frame, a geometric model of the PVC window frame was built, Fig. 4. Model dimensions are shown in Table 2.

The boundary conditions and thermal properties were assumed in accordance with [36] are presented below, in Tables 3 and 4.

Table 2. Frame window model dimensions

Description	Designation	Value, mm
Width of the insulation panel	b_p	191
Width of the window frame	b_f	119
Thickness of the insulation panel (glazing)	d_p	48
Thickness of the window frame	d_f	85

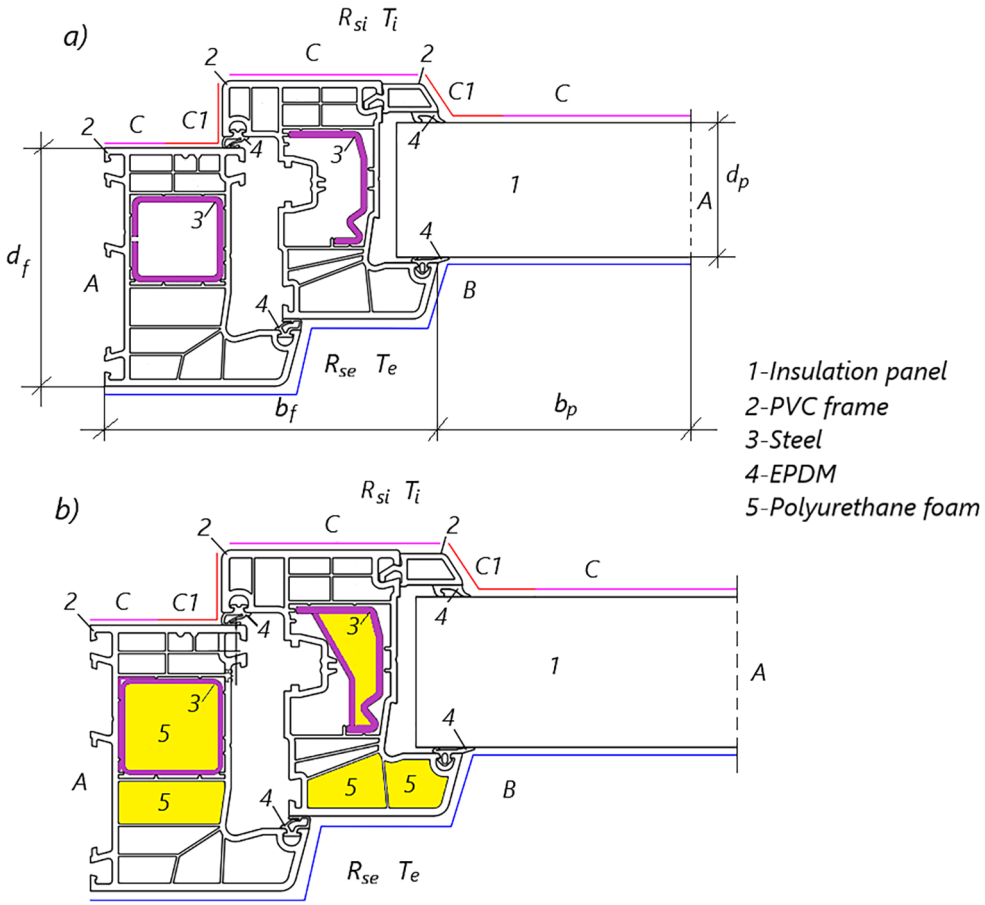

Fig. 4. Window frame with insulation panel-boundary conditions: a) PVC frame with open steel profile; b) PVC frame with closed steel profile and insulation

The equivalent thermal conductivity coefficients k_{eq} for the air-filled PVC profile spaces (air cavities) were determined according to the procedure described in [36]. For the rectangular air cavity, the equivalent thermal conductivity k_{eq} was defined by:

$$k_{eq} = \frac{d}{R_s}, \tag{8}$$

where: d is the air cavity dimension in the heat flow rate direction, and
R_s is the cavity thermal resistance given by:

$$R_s = \frac{1}{h_r + h_{conv}} \tag{9}$$

where: h_{conv} – the convective heat transfer coefficient,
h_r – the „radiative" heat transfer coefficient. These coefficients are defined by:

$$h_{conv} = \begin{cases} \frac{B_1}{d} \; if \; b \leq 5 \text{ mm} \\ max\left(\frac{B_1}{d}, B_2 \, \Delta T_{max}^{1/3}\right) \text{ othewise} \end{cases} \tag{10}$$

$$h_r = 4 \cdot \sigma \cdot F \cdot Em \cdot T_m^3 \tag{11}$$

where: $B_1 = 0.025 \; W/(m \; K)$,
$B_2 = 0.73 \, W/\left(m^2 \; K^{4/3}\right)$,
ΔT_{max} – is the maximum surface temperature difference in the cavity,

Table 3. Boundary conditions

Description	Designation	Thermal surface resistance, m²K/W		Temperature, °C	
Adiabatic conditions	A	∞		-	
Boundary conditions on external side of the model	B	R_{se}	0.04	T_e	0
Boundary conditions on internal side of the model	C/C1	R_{si}	0.13/0.2	T_i	20

Table 4. Thermal properties of the model

Material	Thermal conductivity, W/(m K)	Emissivity	Reference
Insulation panel	0.035	0.9	[36]
PVC	0.17	0.9	[36]
Steel	50	0.6	[36]
EPDM	0.25	0.9	[36]
Polyurethane foam PUR	0.025	0.9	[21]

$\sigma = 5.67 \cdot 10^{-8}\ W/(m^2K^4)$ – the Stefan-Boltzmann constant,
T_m – the average temperature on the boundaries of the cavity.

Surface emittance Em is determined by equation:

$$Em = \left(\frac{1}{\varepsilon_1} + \frac{1}{\varepsilon_2} - 1\right)^{-} \tag{12}$$

where: ε_1 and ε_2 – the emissivity of the surfaces.

View factor F is expressed by formula:

$$F = 0.5 \cdot \left(1 + \sqrt{1 + \left(\frac{d}{b}\right)^2} - \frac{d}{b}\right) \tag{13}$$

where: b – width of the equivalent air cavity.

Non-rectangular cavities are transformed into rectangular cavities of same area and aspect ratio according to defined rules in [36].

Thermal performance

In particular, to evaluate the frame thermal transmittance, the glazing system is replaced by an insulation panel with a thermal conductivity of 0.035 W/(m K) in accordance with the recommendations of the standard [36]. In order to identify the thermal transmittance of the frame U_f, it is necessary to define a thermal coupling coefficient L_{2D} that is the two-dimensional heat transfer coefficient, expressed in W/(mK). The thermal coupling coefficient L_{2D} was determined as follows:

$$L_{2D} = \frac{\Phi_l}{(T_e - T_i)} \tag{14}$$

where: Φ_l – heat flow rate per metre length through the window,
T_e – outdoor temperature,
T_i – indoor temperature.

In turn, the flow rate Φ_l was determined by numerical integration by using trapezoidal rule over interior boundary surface, the heat flux q_n

$$q_n = \frac{T_i - T_{si}}{R_{si}} \tag{15}$$

where: R_{si} – thermal surface resistance on the internal boundary of the model,
T_{si} – surface temperature on the inside boundary of the model.

$$\Phi_l = \frac{1}{2}\sum_{k=1}^{N}(q_n^{k+1} + q_n^k)\Delta l_k \tag{16}$$

where: Δl_k – lenght of the k-th subinterval,
N – number of subintervals on internal side of the model.

The thermal transmittance coefficient of the window frame U_f was determined from the following relationship [36]:

$$U_f = \frac{L_{2D} - U_p \cdot b_p}{b_f} \tag{17}$$

where: L_{2D} – linear thermal coupling coefficient of the frame in W/(m K),
U_p – panel thermal transmittance coefficient,
b_f – panel width. In the analysed case, the thermal transmittance coefficient of the insulation panel was equal to $U_p = 0.64565$ W/ (m^{2}K) and determined on the basis [40]:

$$U_p = \frac{U_{p-p} \cdot b_{p-p} + (b_p - b_{p-p}) \cdot U_{p-n}}{b_p} \tag{18}$$

$$U_{p-p} = \frac{1}{R_p + R_{si-p} + R_{se}} \tag{19}$$

$$U_{p-n} = \frac{1}{R_p + R_{si} + R_{se}} \tag{20}$$

where: $R_p = d_p/k_p$ – panel thermal resistance,
$k_p = 0.035\ W/(m\ K)$ – thermal conductivity of the panel,
b_{p-p} – width of the segment where reduced radiation/convection takes place in edges between two surfaces,
$R_{si-p} = 0.2\ m^2\ K/W$ – internal thermal surface resistance where reduced radiation/convection takes place,
R_{se} – thermal surface resistance on the outer surface,
R_{si} – thermal surface resistance on the internal surface.

In the next stage, a numerical model was built using the finite element method, Fig. 5. The numerical model was built in accordance with the requirements included in the standard [36]. The computational domain was modelled using three-node triangular finite elements and two-node edge elements with a smooth change in mesh density to reduce the risk of numerical errors. The best finite element mesh was determined by performing three simulations for different finite element densities, starting with the mesh with the lowest density and fine-tuning it to the point where the numerical results no longer depended on the size of the finite elements.

To estimate the quality of numerical calculations, the so-called grid convergence index (GCI) was based on Richardson's extrapolation [37]. The GCI Index shows how the computed value is far from the asymptotic numerical value. The grid convergence index was calculated from equation [38]:

$$GCI_{21} = f\ \frac{|e_{1-2}|}{r_{1-2}^{p} - 1} \tag{21}$$

where: $f = 1.25$ – safety factor for comparisons of the at least three grids,
$|e_{1-2}| = |(U_1 - U_2)/U_1|$ – relative error,
r – is the grid refinement factor,
p – is the order of convergence.

The results of the evaluation of the calculations' quality are presented in Table 5.

Based on numerical calculations, the linear thermal coupling coefficient L_{2D} and the frame thermal transmittance coefficient U_f were determined, as shown in Table 6. Below, Figure 6 shows the isotherms in the window frame cross-section and the heat flux density for the two analysed cases. For a window frame with insulation and closed stiffening profiles, the shift of the low temperature zone closer to the outer surface is

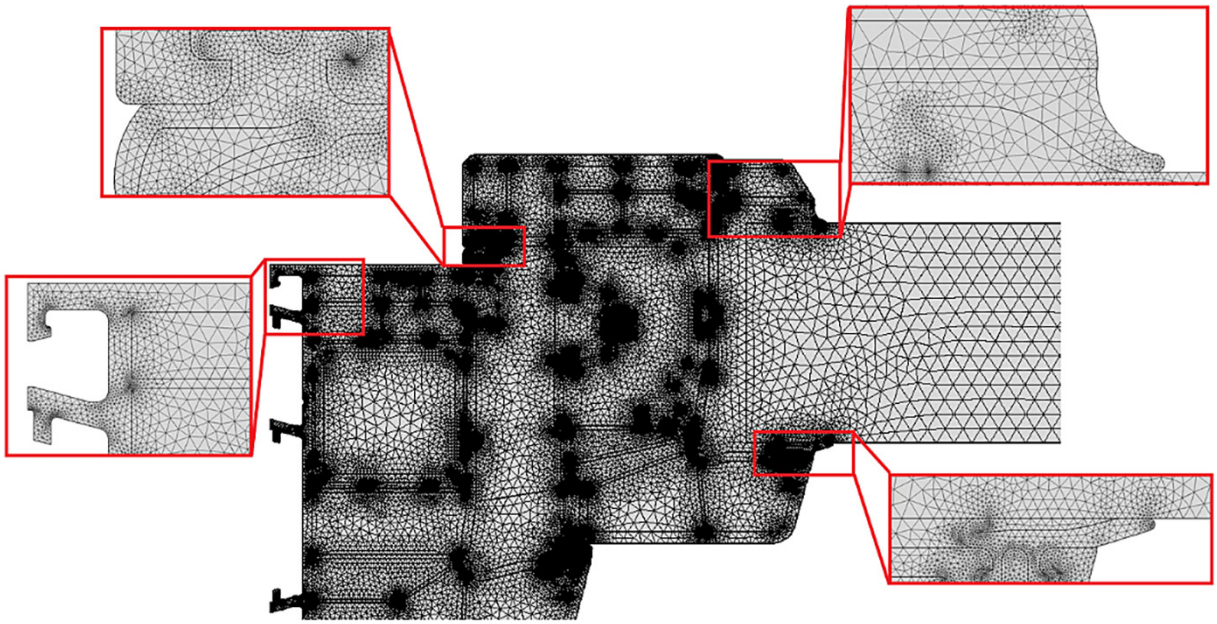

Fig. 5. Finite element grid

Table 5. GCI index for the window frame with closed metal profiles and additional insulation

Grid No.	1	2	3	GCI_{21}, ‰
Number of finite elements	60242	49061	38615	0.1
Frame heat transfer coefficient, U_f, $^{W}/_{(m^2K)}$	1.112627	1.112651	1.112658	

noticeable. A very intense heat transfer through the metal profiles is visible, which is caused by a very high thermal conductivity coefficient. This is evidenced by very high values of the heat flux density. Therefore, it is advisable to replace the windows' metal stiffening profiles with composite profiles with a much lower thermal conductivity coefficient. In addition, the sensitive places through which heat losses are intense are the connection of the shaft with the window frame and the space separating the sash profile from the frame profile.

As shown in the simulation results, filling large air spaces with insulating material allowed the U_f frame thermal transmittance coefficient to be reduced by over 10%. Thus, the use of closed metal profiles that stiffen the window frame, together with additional insulation, improves not only the mechanical, but also the thermal properties of the window. Thermal insulation of the PVC frame reduces the negative energy effect caused by the use of closed metal profiles.

In the next step, the value of the linear thermal transmittance coefficient at the window-wall connection was determined. Two cases were analysed: the first was a window with a PVC frame with open steel stiffening profiles, and the second was a PVC frame with closed steel stiffening profiles and thermal insulation. For this purpose, a geometric model was built, Fig. 7, in accordance with the requirements included in [39]. The geometric dimensions of the model and its thermal properties are presented in Tables 7 and 8. The wall thermal transmittance coefficient U was determined from equation (22) in accordance with [40] and it amounted to:

$$U = 0.188 \frac{W}{(m^2K)}$$

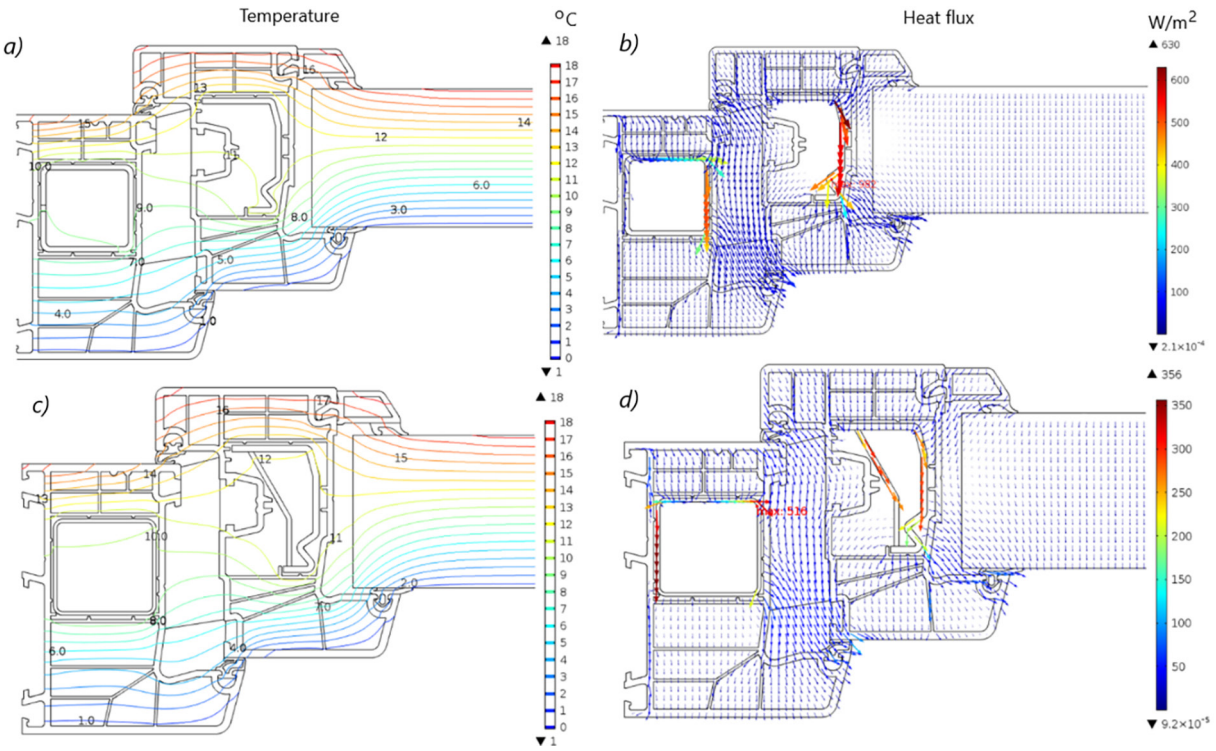

Fig. 6. Temperature distribution of the standard frame and with insulating inserts: a) PVC frame with open steel profile-temperature field, b) PVC frame with open steel profile-heat flux, c) PVC frame with closed steel profile and insulation-temperature field, d) PVC frame with closed steel profile and insulation-heat flux

Tab. 6. Linear thermal coupling coefficient and frame heat transfer coefficient

Model	$L_{2D}, \frac{\mathrm{W}}{(\mathrm{mK})}$	$U_f, \frac{\mathrm{W}}{(\mathrm{m^2K})}$
PVC frame with open stiffening profiles without insulation	0.27098	1.241
PVC frame with closed stiffening profiles and insulation	0.25572	1.113

$$U = \frac{1}{R_{si} + \sum_{j=1}^{N} \frac{d_j}{k_j} + R_{se}} \tag{22}$$

where: d_j – thickness of the of j-th of any homogenous layer which is part of the building component,
k_j – thermal conductivities of these homogenous layers,
N – the number of the layers of the building component,
R_{se} – thermal surface resistance on the external boundary of the building component,
R_{si} – thermal surface resistance on the internal boundary of the building component.

The boundary conditions were adopted as in the previous case, Table 3, and a numerical model was built using the finite element method. The computational domain was created using three-node triangular finite elements and two-node edge elements with a smooth change of mesh density to reduce the risk of numerical errors. As before, the quality of the numerical calculations was assessed using the GCI mesh convergence index and in this case GCI index not exceed 0.5%.

On the basis of numerical calculations, at the given boundary conditions, the temperature field was obtained at the connection of the window with the wall, Fig. 8, and the value of the linear heat transfer coefficient at the connection of the window with the wall was determined using the relationship:

$$\Psi = L_{1-2-3}^{2D} - L_{2-3}^{2D} - U \cdot b_{1-2} \tag{23}$$

where: Ψ – linear thermal transmittance coefficient at the joint of the window frame with the wall,
L_{2-3}^{2D} – linear thermal coupling coefficient of the frame,
L_{1-2-3}^{2D} – linear thermal coupling coefficient of the frame with the wall,
U – wall thermal transmittance coefficient. Linear thermal coupling coefficient L_i^{2D} and heat flow rate per metre length Φ_l was determined using the relationship (14-16).

Table 7. Thermal properties of the wall model

Material	Thermal conductivity, W/mK	Reference
Polyurethane foam PUR	0.025	[21]
Plaster	1.0	[40]
Autoclaved aerated cellular concrete wall	0.35	[40]
Warm windowsill – extruded polystyrene (XPS)	0.036	[40]
Wall insulation – expanded polystyrene (EPS)	0.036	[40]
Lintel-reinforced concrete	1.7	[40]

Table 8. Dimensions of the geometric model of the window-wall connection

Description	Designation	Value, mm
Width of the frame	$b_{2\text{-}3}$	310
Width of the wall	$b_{1\text{-}2}$	1010
Wall thickness	d_{wall}	240
Wall insulation thickness	d_{ins}	160
Internal plaster thickness	d_{oi}	15
External plaster thickness	d_{oe}	5
Width of the lintel	b_t	220

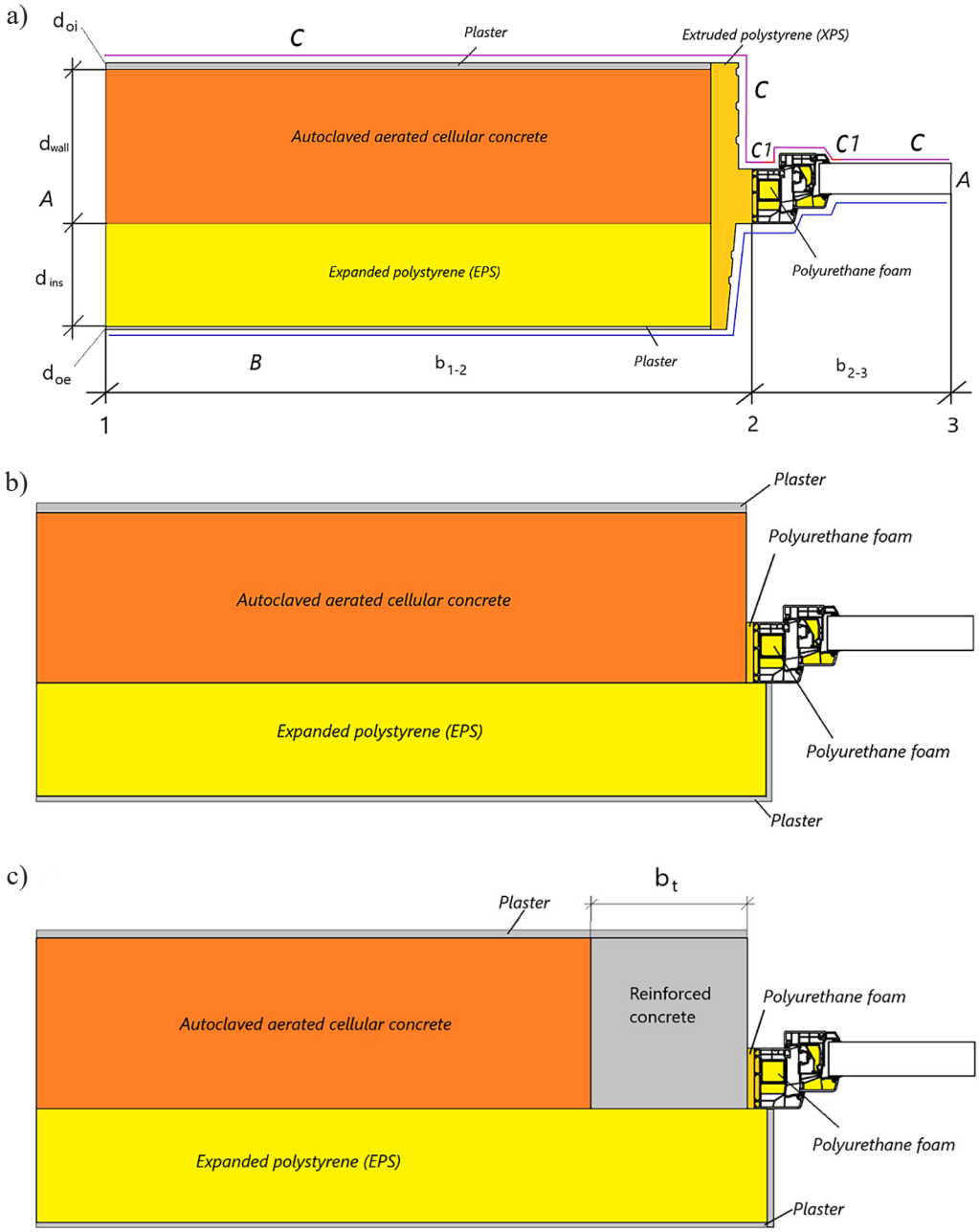

Fig. 7. Connection of the window frame with the wall (a) sill, (b) jamb, (c) lintel

On this basis, the linear thermal transmittance coefficient was determined at the joint of the window with the wall Ψ, Table 9. As can be seen, there is a significant reduction in the influence of linear thermal bridges on heat losses. There was a 9.6%, 1.0% and 3.5% reduction in the value of the linear heat transfer coefficient Ψ in comparison to the frame without insulation, respectively for the window sill, the jamb and the lintel. Thus, the thermal insulation of the PVC frame not only reduces the thermal transmittance coefficient of the U_f frame, but also has a positive effect on reducing the linear thermal bridges at the connection between the window and the wall.

EXPERIMENTAL ANALYSIS

In order to analyse the influence of the insulation in the PVC window frame with closed metal stiffening profiles on the linear thermal bridge at the junction with the glass, experimental tests were conducted. The windows were installed in the wall of the heated measuring chamber, Fig.9.

Measurements were performed under steady-state conditions. During the measurements, the ambient temperature and humidity were recorded by datalogger, Table 10.

The simple and rapid operation of the infrared cameras and a non-invasive measurements

Table 9. Linear heat transfer coefficient at the joint of the window with the wall

Model	$L^{2D}_{1-2-3}, \frac{W}{(mK)}$	$L^{2D}_{2-3}, \frac{W}{(mK)}$	$\Psi, \frac{W}{(mK)}$
PVC frame with open stiffening profiles without insulation – window sill	0.49519	0.27098	0.0343
PVC frame with insulation and closed stiffening profiles – window sill	0.47661	0.25572	0.0310
PVC frame with open stiffening profiles without insulation – jamb	0.49937	0.27098	0.0385
PVC frame with insulation and closed stiffening profiles – jamb	0.48367	0.25572	0.0381
PVC frame with open stiffening profiles without insulation – lintel	0.52588	0.27098	0.0650
PVC frame with insulation and closed stiffening profiles – lintel	0.50829	0.25572	0.0627

way make thermography a widely applied for many years technique in various fields such as for example building [41, 42, 44, 45, 46]. Therefore, in this case, this technique was used to identify linear thermal bridges. A FLIR P640 thermal imaging camera with 640×480 detector resolution, 30 mK thermal sensitivity and 7.5–13 µm spectral range was used to measure the temperature field.

First, the "reflected" temperature, Fig. 10, was measured in accordance with the standard [43]. For this purpose, the average temperature on the "diffusion" mirror surface was measured for the emissivity $\varepsilon = 1$. The reflected temperature, measured in this way, was 24.3 °C.

In order to identify the influence of linear thermal bridges on heat loss through windows, the so-called the incidence factor of the thermal

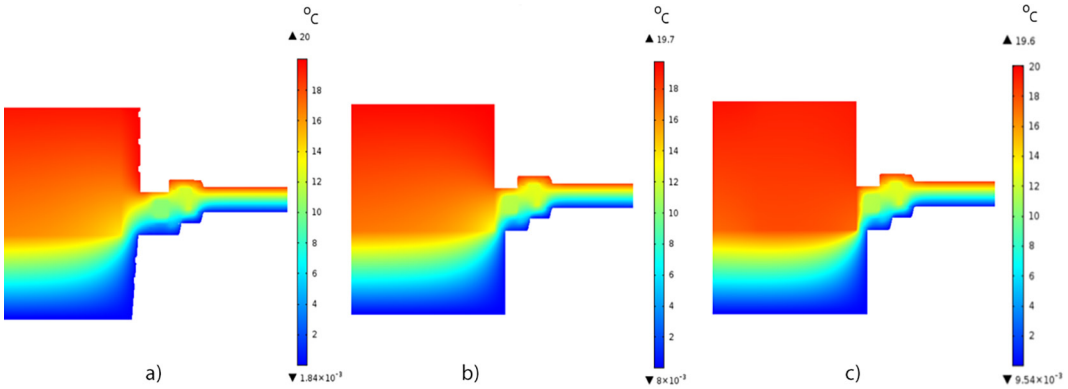

Fig. 8. Temperature distribution at the at the joint of the window with the wall (a) sill, (b) jamb, (c) lintel

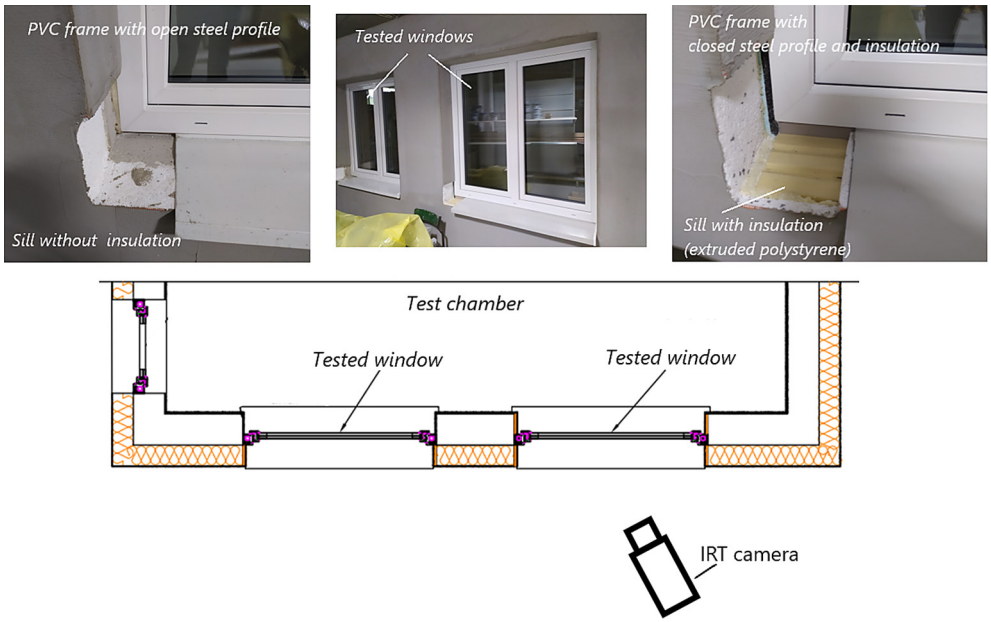

Fig. 9. The test chamber

bridge I_{tb} [44, 45, 46] was utilized, which is defined as follows:

$$I_{tb} = \frac{\sum_{p=1}^{N}\left(T_f - T_{s,p}\right)}{N\left(T_f - T_{sm}\right)}, \quad (24)$$

where: T_f – fluid (environmental) temperature,
$T_{s,p}$ – thermal image temperature of the partition surface along the line,
N-number of pixels,
T_{sm} – surface temperature in the area not affected by the thermal bridge.

The incidence factor of the thermal bridge I_{tb} is defined as the ratio between the heat flow through building component in real conditions (with thermal bridge presence) and the heat flow in absence of the thermal bridge. If there is no thermal bridge then I_{tb} = 1, and if there is thermal bridge, then I_{tb}> 1. Thus, the higher the I_{tb} value, the greater the influence of the thermal bridge on heat losses. There is a relationship between I_{tb} and the linear thermal transmittance coefficient Ψ [44, 45]:

$$I_{tb} = \frac{\Psi + \sum_{j=1}^{K} U_j\, l_j}{\sum_{j=1}^{K} U_j\, l_j} = \frac{U_{tb}\, A}{U\, A} = \frac{U_{tb}}{U}, \quad (25)$$

where: U_j – thermal transmittance coefficient of the j-th component adjacent to the sternum,
l_j – length of the j-th component adjacent to the sternum,

Table 10. Environmental parameters

Measured environmental parameter	Value
Air temperature, T_f	21.7 °C
Relative humidity, *RH*	56%

A-surface area,
U_{tb} – thermal transmittance coefficient taking into account the thermal bridge,
U – thermal transmittance coefficient without taking into account the bridge.

Multiplied the incidence factor of the thermal bridge I_{tb} obtained from the thermal image by the U-value of building component not influenced by thermal bridge U, gives the U-value of a component including thermal bridging U_{tb}:

$$U_{tb} = I_{tb}\, U \quad (26)$$

The incidence factor I_{tb} clearly describes the influence of linear thermal bridges on the heat transport process and its value is proportional to the value of the linear heat transfer coefficient. In order to determine the value of the incidence factor I_{tb}, and, thus, the linear thermal transmittance coefficient Ψ, the temperature was measured from the place of the linear thermal bridge at the junction of the glass pane with the window frame, Fig. 11. Then the temperature values were generated along measurement lines, Fig. 12. The value of the emissivity window glazing, ε = 0.88, in the spectral range operation of the thermal camera was determined on the basis [47, 48] and [49, 50].

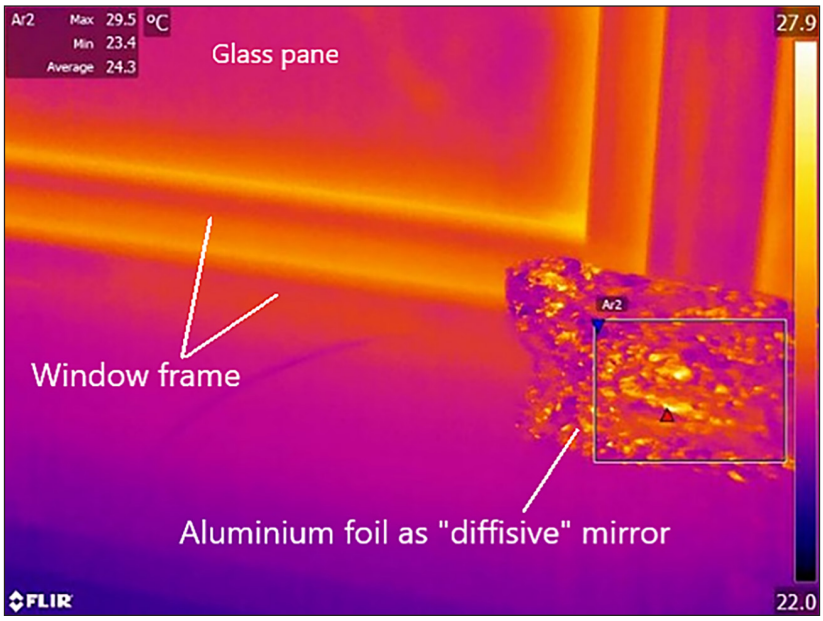

Fig. 10. Measurement of the "reflected" temperature

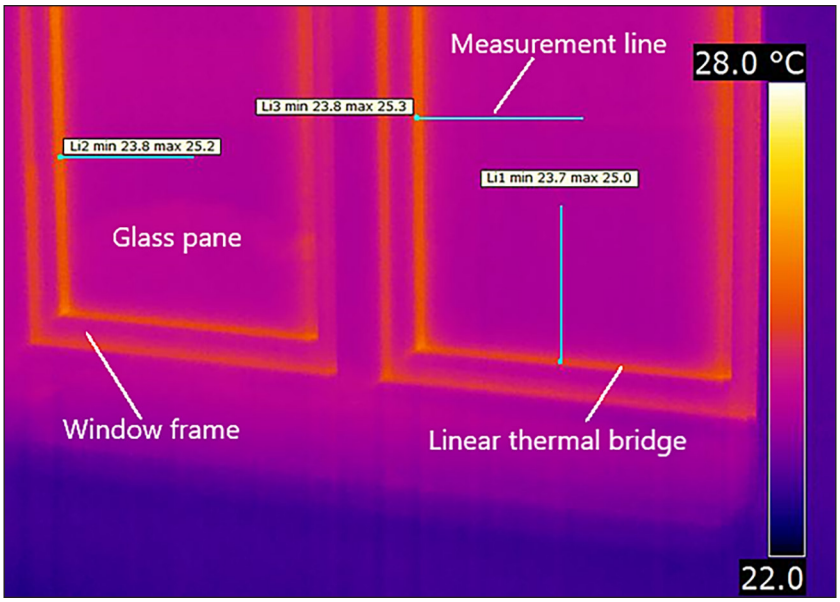

Fig. 11. Thermogram of the tested window

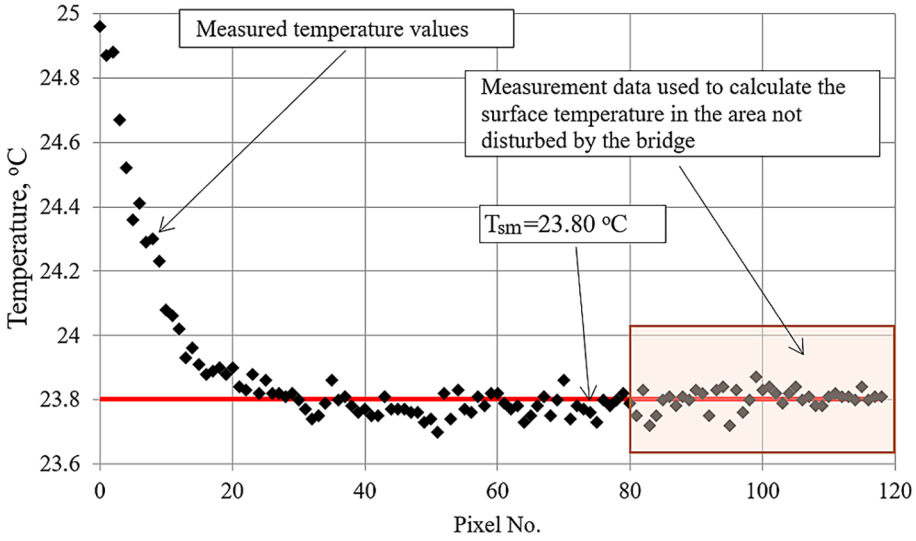

Fig. 12. Temperature distribution along the measurement line on the glass surface

In order to determine the surface temperature in the area not disturbed by the thermal bridge, the arithmetic mean of the line fragment for which the temperature stabilized on the glass surface was calculated. The temperature T_{sm} was calculated as the arithmetic mean:

$$T_{sm} = \sum_{p=1}^{M} T_{s,p} \tag{27}$$

where: M – number of measurement points from an area not affected by the thermal bridge.

Finally, the measurement uncertainty was analysed. The analysis of measurement errors is necessary to give a quantitative description of the validity of the experimental results and therefore an analysis of the uncertainty of the incidence factor I_{tb} was performed. The uncertainty in determining the incidence factor depends on the uncertainties in the parameters which are directly measured. The combined standard uncertainty of the composite quantity $Y = Y(X_1, X_2, \ldots, X_n)$ was calculated according [51, 52] from:

$$u_c(Y) = \sqrt{\sum_{j=1}^{n} \left(\frac{\partial Y}{\partial X_i} u(X_i) \right)^2}, \tag{28}$$

where: $u(X_i)$ −the standard uncertainties of the partial measurements.

The standard uncertainty of the thermal image temperature and emissivity were estimated on the basis [53, 54, 55]. Values of the uncertainties of parameters were presented in Table 11.

As a part of the research, the values of the I_{tb} factor were determined for the window with closed stiffening profiles, Table 12, and additional thermal insulation, and for windows with open stiffening profiles, Table 13.

A lower I_{tb} value for a window with closed stiffening profiles and additional thermal insulation – as compared to open stiffening profiles – indicates a lower linear thermal bridge at the joint between the glass pane and the window frame. The percentage reduction in the value of the linear thermal transmittance coefficient Ψ at the junction of the glass pane with the frame PVC profile is directly proportional to the percentage reduction in the incidence factor I_{tb}. In this case, it amounted to 6.5%.

CONCLUSIONS

The work covers numerical and experimental studies of the energy properties of a window frame made of PVC. In order to increase torsional stiffness and reduce the risk of deformation of the window frame during the window's installation, closed metal profiles have been used to stiffen the PVC frame, which are characterized by much greater torsional stiffness than the commonly used open profiles. In addition, additional thermal insulation of air spaces in the PVC frame was used to improve the thermal properties of the window and reduce the negative energy effect caused by the use of closed metal profiles. The simulation results demonstrated that filling the air cavities with insulating material allowed for a reduction in the thermal transmittance coefficient U_f of the frame by over 10%. Moreover, at the juncture of the window and the wall, there is a reduction in the influence of linear thermal bridges on heat losses.

The reduction of the linear thermal transmittance coefficient Ψ, compared to the frame without insulation, was: 9.7% for the window sill, 1.2%, for jamb, and 3.6% for lintel.

That is, the thermal insulation of the PVC frame not only reduces the thermal transmittance coefficient U_f of the frame, but also has a positive

Table 11. Values of uncertainties

Parameter	Standard uncertainty
Fluid temperature	±0.3 °C
Thermal image temperature	± 1.1 °C
Window glazing emissivity	±0.02
Relative humidity	±5%
Incidence factor	±25%

Table 12. Results of the incidence factor I_{tb} for a window with closed steel stiffening profiles

No.	T_f, °C	$\sum_{p=1}^{M}(T_f - T_p)$, °C	M	T_{sm}, °C	I_{tb}
L1	21.7	-258.30	119	23.80	1.032
L2	21.7	-232.79	102	23.82	1.078
L3	21,7	-300.98	128	23.93	1.056
L4	21,7	-326.29	132	24.02	1.065
L5	21.7	-372.43	151	24.03	1.060
Average				1.058	

Table 13. Results of the incidence factor I_{tb} with open steel stiffening profiles

No.	T_f, °C	$\sum_{p=1}^{M}(T_f - T_p)$, °C	M	T_{sm}, °C	I_{tb}
L1	21.7	-333.18	174	23.36	1.153
L2	21.7	-329.71	172	23.42	1.112
L3	21.7	-294.55	156	23.42	1.100
L4	21.7	-235.16	99	23.84	1.113
L5	21.7	-510.83	196	23.90	1.183
Average				1.132	

effect on reducing the influence of linear thermal bridges at the connection of the window with the wall. It was also found that the incidence factor I_{tb} decreased by more than 6% when the thermal installation was used. Thus, there is also a positive effect on the linear thermal bridge at the joint of the glass pane with the window frame.

Acknowledgements

The works were carried out within the project entitled "Development and implementation into production of an innovative window construction with increase mechanical strength and that minimizes linear thermal bridges" with a number of RPPK.01.02.00-18-0033/18-00 co-financed by the European Regional Development Fund.

REFERENCES

1. Eurostat: https://ec.europa.eu/eurostat/statistics explained/index.php?title=Energy_statistics_-_an_overview#Final_energy_consumption
2. International Energy Agency Report: „Transition to Sustainable Buildings Strategies and Opportunities to 2050", https://www.iea.org/reports/transition-to-sustainable-buildings
3. Directive (EU) 2010/31/EU: https://eur-lex.europa.eu/LexUriServ/LexUriServ.do?uri=OJ:L:2010:153:0013:0035:EN:PDF
4. Directive (EU) 2018/84: https://eur-lex.europa.eu/legal content/EN/TXT/?uri=uriserv:OJ.L_.2018.156.01.0075.01.ENG
5. United nations economic commission for europe joint task force on energy efficiency standards in buildings. Mapping of existing technologies to enhance energy efficiency in buildings in the UNECE Region; UNECE: Geneva, Switzerland, 2019. https://unece.org/fileadmin/DAM/energy/se/pdfs/geee/study/Final_Master_file_-_March_11_final_submission.pdf
6. Berardi U. Building energy consumption in US, EU, and BRIC countries. Procedia Engineering 2015; 118: 128–136.
7. Mangkuto R.A., Rohmah M., DianAsri A. Design optimisation for window size, orientation, and wall reflectance with regard to various daylight metrics and lighting energy demand: A case study of buildings in the tropics. Applied Energy 2016; 164: 211–219.
8. Polish Ministry of Transport, Construction and Maritime Economy. Regulation of the Minister of Transport, Construction and Maritime Economy of 5 July 2013 on the Technical Conditions That Buildings and Their Location Should Satisfy; Polish Ministry of Transport, Construction and Maritime Economy: Warsaw, Poland, 2015.
9. Kotti S., Teli D., James P.A.B. Quantifying Thermal Bridge Effects and Assessing Retrofit Solutions in a Greek Residential Building. Procedia Environmental Sciences 2017; 38: 306–313.
10. Borgero S., Chiari A. The influence of thermal bridge calculation method on the building energy need: a case study. Energy Procedia 2018; 148: 1042–1049.
11. Peel M.C., Finlayson B.L., McMahon T.A. Updated world map of the Koppen-Geiger climate classification. Hydrol. Earth Syst. Sci. 2007; 11: 1633–1644.
12. Evola G., Margani G., Marletta L. Energy and cost evaluation of thermal bridge correction in Mediterranean climate. Energy and Buildings 2011; 43: 2385–2393.
13. Mangkuto R.A., Wang S., Aries M.B.C., van Loenen E.J.,. Hensen J.L.M, Comparison between lighting performance of a virtual natural lighting solutions prototype and a real window based on computer simulation. Frontiers of Architectural Research 2014; 3(4): 2095–2635.
14. Brandt E. Moisture in buildings, SBi Directions 224, 2-nd ed. Copenhagen: Danish Building Research Institute, 2013.
15. Tafakkori R., Fattahi A. Introducing novel configurations for double-glazed windows with lower energy loss. Sustainable Energy Technologies and Assessments 2021; 43: 1–10.
16. Ben-Nakhi A.E. Minimizing thermal bridging through window systems in buildings of hot regions. Applied Thermal Engineering 2002; 22: 989–998.
17. Pelss M., Blumberga A., Kamenders A. Thermal Bridge Impact on the Heating Demand in a Low-Energy House. Environmental and Climate Technologies 2010; 4: 76–81.
18. Bergero S., Cavalletti P., Chiari A. Energy refurbishment in existing buildings: Thermal bridge correction according to DM 26/06/2015 limit values. Energy Procedia 2017; 140: 127–140.
19. Misiopecki C., Bouquin M., Gustavsen A., Jelle B. P. Thermal modelling and investigation of the most energy-efficient window position. Energy and Buildings 2018; 158: 1079–1086.
20. Kim S.H., Jeong H., Soo Cho S. A study on changes of window thermal performance by analysis of physical test results in Korea. Energies 2019; 12: 1–17.
21. Paulos J., Berardi U. Optimizing the thermal performance of window frames through aerogel enhancements. Applied Energy 2020; 266: 1–18.
22. Berardi U., Kisilewicz T., Kim S., Lechowska A., Paulos J., Schnotale J. Experimental and numerical investigation of the thermal transmittance of PVC window frames with silica aerogel. Journal of Building Engineering 2020; 32: 1–12.
23. Van Den Bosschea N., Buffel L., Janssens A. Thermal optimization of window frames. Energy Procedia 2015; 78: 2500–2505.
24. Lechowska A., Schnotale J.A., Baldinelli G. Window frame thermal transmittance improvements without frame geometry variations: An experimentally validated CFD analysis. Energy and Buildings 2017; 145: 188–199.

25. Cannavale A., Martellotta F., Berardi U., Rubino Ch., Liuzzi St., De Carlo V., Ayr U. Modelling of an Aerogel-Based "Thermal Break" for Super-Insulated Window Frames. Buildings 2020; 10(60): 1–15.
26. Abdoli Naser S., Haghparast F., Singery M., Sattari Sarbangholi H. Optimization of thermal performance of windows in intermediate housing in cold and dry climate of Tabriz. Iranian (Iranica) Journal of Energy and Environment 2021; 12: 327–336.
27. Baldinelli G., Bianchi F. Windows thermal resistance: Infrared thermography aided comparative analysis among finite volumes simulations and experimental methods. Applied Energy 2014; 136: 250–258.
28. Barnes B., Pagán-Vázquez A., Liesen R. Window related thermal bridges, thermal performance of the exterior envelopes of whole building. XII International Conference, Clearwater, Florida, USA 2013.
29. Cappelletti F., Gasparella A., Romagnoni P., Baggio P. Analysis of the influence of installation thermal bridges on windows performance: The case of clay block walls. Energy and Buildings 2011; 43: 1435–1442.
30. Ibrahim M., Biwole P.H., Wurtz E., Achard P. Limiting windows offset thermal bridge losses using a new insulating coating. Applied Energy 2014; 123: 220–231.
31. Jakubowicz A., Orłoś Zb. Strength of materials. WNT, 1984. (in Polish)
32. Fang Y., Eames P.C., Hyde T.J., Norton B. Complex multi-material insulating frames for windows with evacuated glazing. Solar Energy 2002; 79: 245–261.
33. Gustavsen A., Grynning S., Arasteh D., Jelle B.P., Goudey H. Key elements of and material performance targets for highly insulating window frames. Energy Build. 2011; 43: 2583–2594.
34. Takada K., Hayama H., Mori T., Kikuta K. Thermal insulated PVC windows for residential buildings: feasibility of insulation performance improvement by various elemental technologies. Journal of Asian Architecture and Building Engineering 2020; 20: 340–355.
35. Gojak M.D., Kijanović A.I., Rudonja N.R., Todorović R.I., Experimental and numerical investigation of thermal improvement of window frames. Thermal Science 2021; 25: 2579–2588.
36. International Standard ISO 10077-2 – Thermal performance of windows, doors and shutters – Calculation of thermal transmittance – Part 2: Numerical method for frames, 2017.
37. Kwaśniewski L. Application of grid convergence index in FE computation. Bulletin of the Polish Academy of Sciences 2013; 61: 123–128.
38. Journal of Fluids Engineering Editorial Policy Statement on the Control of Numerical Accuracy, https://www.asme.org/wwwasmeorg/media/resourcefiles/shop/journals/jfenumaccuracy.pdf
39. International Standard ISO 10211 – Thermal bridges in building construction-Heat flows and Surface temperatures-Detailed calculations, 2017.
40. International Standard ISO 6946, Building components and building elements – thermal resistance and thermal transmittance – calculation method, 2017.
41. Rahman Al-Kassir A., Fernandez J., Tinaut F.V., Castro F. Thermographic study of energetic installations. Applied Thermal Engineering 2005; 25: 183–190.
42. Marino B.M., Muñoz N., Thomas L.P. Estimation of the surface thermal resistances and heat loss by conduction using thermography. Applied Thermal Engineering 2017; 114: 1213–1221.
43. International Standard ISO 18434-1 Condition monitoring and diagnostics of machines – Thermography – Part1: General procedures.
44. Nardi I., Ambrosini D., Paoletti D., Sfarra St. Combining Infrared Thermography and Numerical Analysis for Evaluating Thermal Bridges In Buildings: A Case Study. Int. Journal of Engineering Research and Applications 2015; 5: 67–76.
45. Rüdisser D., Asdrubali F., Baldinelli G., Bianchi F. A quantitative methodology to evaluate thermal bridges in buildings. Third International Conference on Applied Energy, Perugia, Italy 2011: 1241–1252.
46. O'Grady M., Lechowska A., Harte A. M. Infrared thermography technique as an in-situ method of assessing heat loss through thermal bridging. Energy and Buildings 2017; 135: 20–32.
47. McLeod R.S., Wagner W., Hopfe C.J. Numerical derivation and validation of the angular, hemispherical and normal emissivity and reflectivity of common window glass. Building and Environment 2022; 207: 1–20.
48. Bałon P., Rejman E., Smusz R., Kiełbasa B. Experimental tests of window joinery in the scope of meeting technical requirements. Mechanik 2022; 8–9
49. Uhryński A., Bembenek M. The thermographic analysis of the agglomeration process in the roller press of pillow-shaped briquettes. Materials 2022.
50. Bembenek M., Uhryński A. The use of thermography to determine the compaction of a saddle-shaped briquette produced in an innovative roller press compaction unit. Acta Mechanica et Automatica 2022.
51. Coleman H.W., Steele W.G. Experimentation, Validation, and Uncertainty Analysis for Engineers, third ed. John Wiley & Sons, Inc, 2009.
52. Evaluation of measurement data – Guide to the expression of uncertainty in measurement, GUM, 2008.
53. Muniz P. R., de Araújo Kalid R., Cani S. P. N., da Silva Magalhãe R. Handy method to estimate uncertainty of temperature measurement by infrared thermography. Optical Engineering 2014; 53: 1–7.
54. Bałon P., Rejman E., Smusz R., Kiełbasa, Influence of the shape of reinforcing window profiles on the strength and torsional stiffness of windows. Mechanik 2022; 8–9.
55. Bałon P., Rejman E., Smusz R., Kiełbasa. Comparison of the open and closed profile in the PVC profiles of a window frame. Mechanik 2022; 7.